Using quantum dynamics simulations to follow the competition between charge migration and charge transfer in polyatomic molecules

K. E. Spinlove[a,b], M. Vacher[b,d], M. Bearpark[b], M. A. Robb[b], G. A. Worth[a,c]

[a]*School of Chemistry, University of Birmingham, Birmingham, B15 2TT, U.K.*
[b]*Dept. of Chemistry, Imperial College London, South Kensington, SW7 2AZ, U.K.*
[c]*Dept. of Chemistry, University College London, 20, Gordon St., WC1H 0AJ, U.K.*
[d]*Dept. of Chemistry, Uppsala University, Lägerhyddsvǧen 1, 751 21 Uppsala, Sweden*

Abstract

Recent work, particularly by Cederbaum and co-workers, has identified the phenomenon of charge migration, whereby charge flow occurs over a static molecular framework after the creation of an electronic wavepacket. In a real molecule, this charge migration competes with charge transfer, whereby the nuclear motion also results in the re-distribution of charge. To study this competition, quantum dynamics simulations need to be performed. To break the exponential scaling of standard grid-based algorithms, approximate methods need to be developed that are efficient yet able to follow the coupled electron-nuclear motion of these systems. Using a simple model Hamiltonian based on the ionisation of the allene molecule, the performance of different methods based on Gaussian Wavepackets is demonstrated.

Keywords: Charge Migration, Charge Transfer, Quantum Dynamics Simulation, MCTDH, GWP Method, Ehrenfest Dynamics

1. Introduction

The movement of electronic density in molecules is fundamental to chemistry. *Charge transfer* in which an electron (or hole) moves from one part of the molecule to another due to the change in molecular geometry, i.e. due to nuclear motion, is well-known. More recently, *charge migration* has been found to occur in which the electron density moves, typically after ionisation, over a static nuclear framework [1, 2]. It is due to the fact that a number of eigenstates of the ion contain contributions from the molecular orbital from which the electron is removed. This coupling between the non-stationary electronic wavepacket created by the ionisation leads to motion of the charge. It has been

demonstrated, e.g. in the outer shell ionisation of peptides [3, 4]. A Scheme has also been devised to control the migration using ultrashort (attosecond) laser pulses [5].

Charge migration happens on the few femto-second timescale, faster than nuclear motion. As a result, much of the work on charge migration to date has been performed using static nuclei and questions remain on the competition between it and the charge transfer caused by the nuclear motion, e.g. the nature and timescale of the transition between the two regimes. This transition and subsequent time-evolution is important in understanding processes such as the fragmentation of peptides after ionisation [6, 7, 8].

To study the motion of coupled nuclear and electronic wavepackets it is necessary to solve the time-dependent Schrödinger equation (TDSE). The usual procedure is to first solve the electronic Schrödinger equation at fixed nuclear geometries and set up global potential energy surfaces over which the nuclei move. The TDSE can then be solved (numerically) exactly using a basis set expansion that effectively discretise the evolving nuclear wavefunction on a grid [9, 10].

It is well known that solving the TDSE scales exponentially with the number of degrees of freedom. Efficient algorithms are required for molecules with more than a few degrees of freedom. The multi-configurational time-dependent Hartree (MCTDH) method, developed by Meyer, Manthe and Cederbaum [11] has established itself as the most powerful and general scheme for accurate solutions of the TDSE for polyatomic molecules [11, 12, 13]. Using this method, and recent developments such as multi-layer MCTDH [14, 15], accurate quantum dynamics simulations of highly quantum mechanical phenomena such as vibronic coupling [16] and charge transfer [17] have been performed for systems with up to 100 degrees of freedom.

The main bottleneck for quantum dynamics simulations is now providing accurate and flexible molecular potential energy surfaces. This is impossible for grid-based methods as it would require the calculation of many thousands of energies and non-adiabatic couplings at geometries covering configuration space using high level quantum chemistry methods followed by a multi-dimensional fit of appropriate functions to the points. For this reason there is presently much interest in what are termed direct dynamics methods in which the potential surfaces are calculated on-the-fly only where needed by the evolving wavepacket [18]. Ideal for such calculations are methods based on Gaussian wavepackets. These functions are localised in coordinate space and thus can take advantage of the information from quantum chemistry calculations. Many algorithms have been developed over the last few years for such calculations, including the Ab-Initio Multiple Spawning (AIMS) method of Ben-Nun and Martinez [19], the ab initio Multi-Configurational Ehrenfest method (AI-MCE) of Shalashilin [20], and the Direct Dynamics variational Multi-Configurational Gaussian (DD-vMCG) of Worth, Robb and Burghardt [21].

The vMCG method is a fully variational solution of the TDSE using a basis set of Gaussian functions and is based on a variant of MCTDH [22, 23]. It belongs to a class of methods referred to as *Gaussian WavePacket* (GWP)

propagation, but unlike the majority of GWP methods it does not use classical trajectories for the evolution of the basis functions. It has been shown to have good convergence properties and is able to treat non-adiabatic dynamics [24]. This makes it ideal as a direct dynamics method.

The study of charge migration often starts with a short (attosecond) pulse that ionises a molecule. The band-width of such pulses is wide - of the order of a few eV. This is a challenge for methods that explicitly calculate all states and couplings as the number of states to be included may be large. Ehrenfest methods provide an alternative approach that calculates all the non-adiabatic couplings along a nuclear trajectory and provides only a single mean-field potential surface for the nuclear motion. Recently Ehrenfest trajectories have been used to study the charge migration in benzene [25], glycine [26] and toluene [27].

Ehrenfest trajectories run over a potential surface which is an average of the manifold of surfaces, weighted by the electronic population of the states. They, however, ignore coupling between trajectories loosing the coherence of the nuclear wavepacket. The Multi-Configurational Ehrenfest (MCE) method of Shalashilin uses coupled coherent states, which are related to GWPs, to include the lost coupling [28, 29].

In this paper, a family of GWP-based quantum dynamics methods related to vMCG will be presented. Starting from vMCG, a Multi-Configurational Ehrenfest method is then derived that connects the methods, and shows the approximations being made in this approach.

To test the different levels of theory set up, a simple model with competing charge migration and charge transfer is set up and the population dynamics obtained using the different approaches compared to benchmark MCTDH calculations. The model is based on the ionisation of allene, a small organic molecule (C_3H_4) that has been used in previous studies of charge transfer [30, 31]. With 15 degrees of freedom and strong non-adiabatic coupling, it provides a suitable challenge for quantum dynamics methods.

The paper is organised as follows. The MCTDH method is briefly introduced in Sec. 2.1. In Sec. 2.2 the vMCG method is introduced and variants are derived, showing the relationship between the different levels of theory. There are 3 variants in addition to the full variational solution. The first uses classical Gaussians in place of the full variational basis functions and is termed clMCG. The second completely ignores coupling between the basis functions, leading to a swarm of classical trajectories and is called iMCG. The final uses stationary basis functions that form a grid and is called gMCG.

A number of GWP based approaches to quantum dynamics are in the literature. The clGWP formulation is similar in approach to a number of GWP based methods which use basis functions driven by classical trajectories. These include the spawning method of Martinez [32], the coupled-coherent states of Shalashilin [33] and the periodic projection method of Habershon [34]. The matching pursuit of Wu and Batista [35] and basis expansion leaping of Koch and Frankcombe [36] lie between clMCG and gMCG, using a time-independent basis that is periodically moved to expand the evolving wavepacket. The GBFs of the vMCG method itself move along non-classical trajectories, reminiscent

3

of the quantum trajectories of Bohmian mechanics exemplified by the work of Garaschuk [37] and Curchod and Tavernelli [38].

In Sec. 2.3 the MCG ansatz is transformed into an MCE ansatz and new approximate equations of motion derived, called eMCG, with classical basis functions that each follow an Ehrenfest potential. It is then shown that removing the coupling to provide a swarm of Ehrenfest trajectories is equivalent to the iMCG method. The eMCG method is similar to Shalashilin's multi-configurational Ehrenfest method [29], but derived from a variational approach so clearly showing the approximations being made. The Ehrenfest schemes with mutual coupling between nuclear and electronic functions have the same spirit as the exact factorisation methods of Gross [39] and Cederbaum [40].

The allene model is then described in Sec. 2.4. The results of simulations are divided into two parts. In the first, Sec. 3.1 the state populations of the model from MCTDH calculations are examined to show the damping of the charge migration signal by the nuclear motion. In Sec. 3.2 the results from the different levels of theory are presented to show how the different approximations perform in reproducing the coupled electronic-nuclear dynamics.

2. Theory and Computational Methods

In the following, units are used in which $\hbar = 1$ and the time-dependent Schrödinger Equation is written

$$i\frac{\partial}{\partial t}\Psi(\mathbf{x},\mathbf{r}) = \hat{H}\Psi(\mathbf{x},\mathbf{r}) \quad , \tag{1}$$

where $\mathbf{x}$, $\mathbf{r}$ are the nuclear and electronic coordinates respectively.

2.1. Quantum Dynamics: the MCTDH method

The multi-configurational time-dependent Hartree method (MCTDH) [11] is an established algorithm for solving the TDSE, Eq. (1), for multi-dimensional problems. A particular advantage is good convergence with basis set size, due to its variational foundation. Details of the method are given in the review [12] and monograph [41]. In the following, the single-set version is used in which the wavefunction ansatz uses one set of time-dependent basis functions, φ, known as single-particle functions (SPFs), for all electronic states:

$$\Psi(\mathbf{x},t) = \sum_{j_1 \ldots j_p, s} A_{j_1 \ldots j_p s}(t)\varphi_{j_1}^{(1)}(x_1,t)\ldots\varphi_{j_p}^{(p)}(x_p,t)|s\rangle \quad . \tag{2}$$

There are p sets of functions $\varphi^{(\kappa)}$, with coordinates x_κ, which may be more than one physical coordinate. The electronic states are described by time-independent state vectors, $|s\rangle$. $A_{j_1 \ldots j_p, s}$ are the expansion coefficients. Note that the final index s runs over the electronic states.

4

Equations of motion (EOM) for the SPFs and the expansion coefficients are derived by solving the TDSE using the Dirac-Frenkel variational principle with the ansatz Eq. (2). These are

$$i\dot{A}_{Kt} = \sum_{J,s} \langle \Phi_K t | H | \Phi_J s \rangle A_{J,s} \tag{3}$$

$$i\dot{\varphi}_j^{(\kappa)} = \sum_{ik} \rho_{ji}^{-1}(1-P)\mathcal{H}_{ik}^{(\kappa)}\varphi_k^{(\kappa)} \tag{4}$$

where a multi-index $J = j_1 \ldots j_p$ and a configuration function $\Phi_J = \varphi_{j_1}^{(1)} \ldots \varphi_{j_p}^{(p)}$ have been used for compactness; ρ_{ij} is the reduced density matrix for DOF κ; $\mathcal{H}_{ij}^{(\kappa)}$ the mean-field matrix operator that couples the motion of the sets of SPFs; and P is the projector on to the space spanned by the SPFs. By construction, the SPFs are orthonormal at all times.

2.2. Quantum Dynamics using Gaussian Basis Functions

In the standard MCTDH method, the SPFs are described by time-independent grid-based functions, such as DVRs,

$$\varphi_j(t) = \sum_a c_{aj}(t)\chi_a \quad . \tag{5}$$

It is possible to replace the grid-based SPFs by parametrised Gaussian basis functions (GBFs) and obtain variational EOM for the GBF parameters. This is the G-MCTDH method [22]. GBFs may be more efficient than grid-based functions as they can describe more DOFs in a single particle [42]. In the limit that a single-set of multi-dimensional GBFs are used for the nuclear wavefunction, the method is called the variational multi-configurational Gaussian (vMCG) [23].

The single-set vMCG ansatz is

$$\Psi(\mathbf{x}, t) = \sum_{j,s} A_{j,s}(t)g_j(\mathbf{x}, t)|s\rangle \tag{6}$$

where the second index, s, is related to the electronic state, $|s\rangle$, and with the GBFs,

$$g_j(\mathbf{x}, t) = \exp\left(\sum_\alpha \zeta_{j\alpha}x_\alpha^2 + \xi_{j\alpha}(t)x_\alpha + \eta_j(t)\right) \quad , \tag{7}$$

defined by 3 sets of complex parameters: quadratic, $\boldsymbol{\zeta}$, linear, $\boldsymbol{\xi}$, and scalar, η. Note that the quadratic parameters, which define the width of the GBF, are kept time-independent. This is not strictly necessary, but simplifies the numerics of the problem. A GBF thus corresponds to what is often called a frozen Gaussian wavepacket (GWP).

GWPs were introduced by Heller [43] and have the form:

$$G_j(\mathbf{x}, t) = \exp\left(\sum_\alpha -\sigma_{j\alpha}(x_\alpha - q_{j\alpha}(t))^2 + ip_{j\alpha}(t)(x_\alpha - q_{j\alpha}(t)) + i\gamma_j(t)\right) \tag{8}$$

which is defined by the real parameters $\mathbf{q}$ and $\mathbf{p}$ that are the coordinates and momenta of the centre of the GWP, and the real parameter $\boldsymbol{\gamma}$ that defines the phase. The linear GBF parameters, which are directly related to the variational determination of the system time-evolution, are related to the centre coordinates and momenta of the related GWP by

$$\xi_{j\alpha} = -2\zeta_{j\alpha}q_{j\alpha} + ip_{j\alpha} \tag{9}$$

EOM for the expansion coefficients and GBF linear parameters are again obtained using the Dirac-Frenkel variational principle

$$i\dot{A}_{k,t} = \sum_{js} S_{k,i}^{-1} \left(\langle g_i t | H | g_j s \rangle - i\tau_{ij} \right) A_{j,s} \tag{10}$$

$$i\dot{\xi}_{k\beta} = \sum_{i} C_{k\beta j\alpha}^{-1} Y_{j\alpha} \tag{11}$$

The tensors C and Y are:

$$C_{i\alpha,j\beta} = \rho_{ij} \left(S_{ij}^{(\alpha\beta)} - \sum_{kl} S_{ik}^{(\beta 0)} S_{kl}^{-1} S_{kj}^{(0\alpha)} \right) \tag{12}$$

$$Y_{i\alpha} = \sum_{j} \left(\langle \mathcal{H}_{ij}^{(\alpha 0)} \rangle_{ij} - \sum_{kl} S_{ik}^{(\alpha 0)} S_{kl}^{-1} \langle \mathcal{H}_{lj} \rangle_{ij} \right) \quad , \tag{13}$$

where following matrices have been defined as

$$S_{ij} = \langle g_i | g_j \rangle \quad ; \quad \tau_{ij} = \langle g_i | \dot{g}_j \rangle \tag{14}$$
$$\rho_{ij} = \sum_{s} A_{is}^* A_{js} \quad ; \quad \langle \mathcal{H}_{ik} \rangle_{jk} = \sum_{st} A_{is}^* \langle g_j s | H | g_k t \rangle A_{kt} \quad .$$

along with matrix elements involving derivatives of a GBF with respect to one of its linear parameters:

$$S_{ij}^{(\alpha\beta)} = \langle \frac{\partial g_i}{\partial \xi_{i\alpha}} | \frac{\partial g_j}{\partial \xi_{j\beta}} \rangle \qquad ; \qquad S_{ij}^{(\alpha 0)} = \langle \frac{\partial g_i}{\partial \xi_{j\alpha}} | g_j \rangle \quad ;$$

$$\langle \mathcal{H}_{ij}^{(\alpha 0)} \rangle_{ij} = \sum_{st} A_{is}^* \langle \frac{\partial g_i}{\partial \xi_{j\alpha}} s | H | g_j t \rangle A_{jt} \quad . \tag{15}$$

Use is also made of the time-derivative of a GBF in terms of its time-dependent parameters, ξ and η:

$$|\dot{g}_j\rangle = \sum_{\beta} |\frac{\partial g_j}{\partial \xi_{j\beta}}\rangle \dot{\xi}_{j\beta} + |g_j\rangle \dot{\eta}_j \quad \Rightarrow \quad \langle g_i | \dot{g}_j \rangle = \sum_{\beta} S_{ij}^{(0\beta)} \dot{\xi}_{j\beta} + S_{ij} \dot{\eta}_j \tag{16}$$

The scalar parameters are undefined by the variational principle. A sensible choice is to keep the related GWP normalised and phaseless (i.e. $\gamma = 0$) using the equation

$$\dot{\eta}_k = \sum_{\alpha} -2\sigma_{j\alpha}q_{j\alpha}\dot{q}_{j\alpha} - ip_{j\alpha}\dot{q}_{j\alpha} - iq_{j\alpha}\dot{p}_{j\alpha} \quad . \tag{17}$$

In principle, however, a different choice can be made and the GBFs will remain normalised as long as the diagonal elements of the right time-derivative overlap matrix, τ_{kk}, are purely imaginary, i.e.

$$i\tau_{kk} = \epsilon_k \tag{18}$$

with ϵ_k a real number.

The vMCG method is fully variational, with coupling between the GBFs. This leads to fast convergence and the ability to capture quantum properties such as curve crossing and tunneling in a straightforward manner. For details see the recent review [24]. However, the coupling between the GBFs is expensive on computational resources due to the need to invert the large $\mathbf{C}$ tensor that has dimensions $(n \times f)^2$, where n is the number of GBFs and f the number of DOFs. The method can also be numerically unstable as, like all GBF based methods linear dependencies in the basis functions can occur which result in singularities of the inverse of the overlap matrix. In practice these instabilities can be controlled by numerical techniques such as regularisation.

Other more approximate schemes, referred to as levels of theory, can now be defined that may be computationally more efficient. In the first, it has been noted that the $\mathbf{Y}$ tensor can be expanded in moments of the GBFs [22, 24] i.e.

$$\langle x^n \rangle_{ij} = \langle g_i | x^n | g_j \rangle \tag{19}$$

and Eq. (11) rewritten as

$$\dot{\xi}_{k\alpha} = -2\zeta_{k\alpha}\dot{q}_{k\alpha} + i\dot{p}_{k\alpha} = \left(-2\zeta_{k\alpha}\frac{p_{k\alpha}}{m_\alpha} - i\frac{\partial V}{\partial x_\alpha} \big|_{\mathbf{x}=\mathbf{q}} \right) + C^{-1}_{k\beta j\alpha}Y_{R,j\alpha} \tag{20}$$

$$= X_{k\alpha} + C^{-1}_{k\beta j\alpha}Y_{R,j\alpha} \tag{21}$$

where $Y_{R,j\alpha}$ contains all terms with GBF moments of second order and higher and the second line defines the complex vector $\mathbf{X}$ that contains the classical parts. In the classical multi-configurational Gaussian (clMCG) method these higher order terms are ignored and the GBFs follow classical trajectories

$$\dot{\xi}_{k\alpha} = X_{k\alpha} = -2\zeta_{k\alpha}\frac{p_{k\alpha}}{m_\alpha} - i\frac{\partial V}{\partial x_\alpha} \big|_{\mathbf{x}=\mathbf{q}} \quad . \tag{22}$$

The coefficients retain the full variational character of Eq. (10). Thus the wavefunction is fully quantum mechanical but due to the classical character of the basis set the convergence may be slow and certain phenomena, such as tunelling, may be hard to describe.

A more severe approximation, that loses the full quantum character of the wavepacket, is to use classical GBFs and also ignore the overlap between GBFs. This decouples the GBFs, resulting in the independent multi-configurational Gaussian (iMCG) method. The EOM are

$$i\dot{A}_{k,t} = \sum_s \left(\langle g_k t | H | g_k s \rangle - i\tau_{kk} \right) A_{ks} \tag{23}$$

$$\dot{\xi}_{k\alpha} = -2\zeta_{k\alpha}\frac{p_{k\alpha}}{m_\alpha} - i\frac{\partial V}{\partial x_\alpha} \big|_{\mathbf{x}=\mathbf{q}} \tag{24}$$

7

i.e. the GBFs follow classical trajectory and the "expansion coefficients" are a phase due to the energy along the trajectory. This is a swarm of classical trajectories with Gaussian widths, and the widths only play a role determining the initial weights of the trajectories and the representation of the wavepacket for analysis.

The final level uses time-independent GBFs so that the basis functions form a static grid. This is referred to as gMCG. It has the full quantum dynamical EOM for the expansion coefficients, Eq. (10) and for the GBFs

$$\dot{\xi} = 0 \tag{25}$$

The various levels of theory are summarised in Table 1. It should be noted that the vMCG method is only fully quantum mechanical if the Hamiltonian matrix elements are evaluated completely. In practice, a local harmonic approximation (LHA) of the PES is made at the centre of each GBF which allows the matrix elements to be evaluated analytically.

2.3. Multi-Configurational Ehrenfest Dynamics

To separate out the electronic and nuclear motion further, it is possible to reconfigure the vMCG ansatz into an Ehrenfest-like approach. Introducing the electronic functions

$$|\psi_j(x_{el}, t)\rangle = \sum_s c_{js}(t)|s\rangle \tag{26}$$

the vMCG ansatz can be re-written

$$\Psi(\mathbf{x}, t) = \sum_j B_j(t)g_j(\mathbf{x}, t)|\psi_j(x_{el}, t)\rangle \tag{27}$$

with

$$A_{js} = B_j c_{js} \quad . \tag{28}$$

The Dirac-Frenkel variational principle

$$\langle \delta\Psi | i\frac{\partial}{\partial t} - H | \Psi \rangle = 0 \tag{29}$$

is then applied to the ansatz Eq. (27) to obtain

$$\sum_j iS_{ij}\dot{B}_j = \sum_j \left(H_{ij} - iS_{ij}^{el}\tau_{ij}^g - iS_{ij}^g\tau_{ij}^{el} \right) B_j \tag{30}$$

$$\sum_{j\beta} i\rho_{ij}S_{ij}^{el}S_{ij}^{(\alpha\beta)}\dot{\xi}_{j\beta} = \sum_j \left(\rho_{ij}H_{ij}^{(\alpha 0)} - i\rho_{ij}\tau_{ij}^{el}S_{ij}^{(\alpha 0)} - iB_i^*S_{ij}^{el}S_{ij}^{(\alpha 0)}\dot{B}_j \right) \tag{31}$$

$$\sum_j i\rho_{ij}S_{ij}^g|\dot{\psi}_j\rangle = \sum_j \left(\rho_{ij}H_{ij}^g - i\rho_{ij}\tau_{ij}^g - iB_i^*S_{ij}^g\dot{B}_j \right)|\psi_j\rangle \tag{32}$$

Model	EOM for coefficients	EOM for GBF parameters	full solution TDSE	variational basis	time-dependent basis
MCG ansatz	$\Psi = \sum A_{is} g_i \lvert s \rangle$				
vMCG	$i\dot{\mathbf{A}} = \mathbf{S}^{-1}(\mathbf{H} - i\boldsymbol{\tau})\mathbf{A}$	$i\dot{\xi} = \mathbf{X} + \mathbf{C}_R^{-1}\mathbf{Y}_R$	y	y	y
clMCG	$i\dot{\mathbf{A}} = \mathbf{S}^{-1}(\mathbf{H} - i\boldsymbol{\tau})\mathbf{A}$	$i\dot{\xi} = \mathbf{X}$	y	n	y
iMCG	$i\dot{A}_j = (H_{jj} - i\tau_{jj})A_j$	$i\dot{\xi}_j = X_j$	n	n	y
gMCG	$i\dot{\mathbf{A}} = \mathbf{S}^{-1}(\mathbf{H} - i\boldsymbol{\tau})\mathbf{A}$	$i\dot{\xi} = 0$	y	n	n
MCE ansatz	$\Psi = \sum B_i g_i \psi_i$				
veMCG	$i\dot{\mathbf{B}} = \mathbf{S}^{-1}(\mathbf{H} - i\mathbf{S}^{el}\boldsymbol{\tau}^g - i\mathbf{S}^g\boldsymbol{\tau}^{el})$	$i\dot{\xi}_i = X_i + \mathbf{C}_R^{-1}\mathbf{Y}_R + T^{el}$ $i\dot{\psi}_i = H_{el}(q_i)\psi_i$	y	y	y
eMCG	$i\dot{\mathbf{B}} = \mathbf{S}^{-1}(\mathbf{H} - i\mathbf{S}^{el}\boldsymbol{\tau}^g - i\mathbf{S}^g\boldsymbol{\tau}^{el})$	$i\dot{\xi}_i = X_i$ $i\dot{\psi}_i = H_{el}(q_i)\psi_i$	y	n	y

Table 1: Summary of levels of theory showing which terms are included in the equations of motion (EOM) for the expansion coefficients and Gaussian basis function (GBF) parameters. For an explanation of the terms see the text around Eqs. (10) and (21).

by making variations of a coefficient, δB_i, a linear parameter of a GBF, $\delta \xi_{i\alpha}$, and an electronic function, $\delta \psi_i$, respectively. The notation for the matrix elements:

$$S_{ij}^{el} = \langle \psi_i | \psi_j \rangle \quad ; \quad S_{ij}^{g} = \langle g_i | g_j \rangle \quad ; \quad S_{ij} = \langle \psi_i g_i | \psi_j g_j \rangle \tag{33}$$
$$\tau_{ij}^{el} = \langle \psi_i | \dot{\psi}_j \rangle \quad ; \quad \tau_{ij}^{g} = \langle g_i | \dot{g}_j \rangle \quad ; \quad \rho_{ij} = B_j^* B_j$$
$$H_{ij}^{el} = \langle \psi_i | H | \psi_j \rangle \quad ; \quad H_{ij}^{g} = \langle g_i | H | g_j \rangle \quad ; \quad H_{ij} = \langle \psi_i g_i | H | \psi_j g_j \rangle$$

has been used in an extension of the matrices defined above in Eqs. (15) - (16).

Note that both the electronic functions and GBFs are taken to be normalised but not orthogonal, i.e.

$$S_{ij}^{el} = \langle \psi_i | \psi_j \rangle \quad = \quad 1 \quad i = j \tag{34}$$
$$= \quad \sum_s c_{is}^* c_{js} \quad i \neq j \tag{35}$$

The Eqs. (30) - (32) are coupled. Following the spirit of vMCG, Eq (30) gives immediately an equation of motion for the coefficients

$$i\dot{B}_k = \sum_{ij} S_{ki}^{-1} \left(H_{ij} - iS_{ij}^{el}\tau_{ij}^{g} - iS_{ij}^{g}\tau_{ij}^{el} \right) B_j \tag{36}$$

which, after multiplying by B_l^*, can be substituted back into Eq. (31) to give an equation of motion for the linear GBF parameters

$$i\dot{\xi}_{k\beta} = \sum_{ij\alpha} C_{k\beta,i\alpha}^{-1} \left(Y_{i\alpha} - iS_{ij}^{(\alpha 0)}\tau_{ij}^{el} - i\sum_{lm} S_{il}^{el} S_{il}^{(\alpha 0)} S_{lm}^{-1} S_{mj}^{g} \tau_{mj}^{el} \right) \tag{37}$$

with the C and Y tensors altered from vMCG

$$C_{i\alpha,j\beta} = \rho_{ij} \left(S_{ij}^{el} S_{ij}^{(\alpha\beta)} - \sum_{kl} S_{ik}^{el} S_{ik}^{(\beta 0)} S_{kl}^{-1} S_{kj}^{(0\alpha)} S_{kj}^{el} \right) \tag{38}$$

$$Y_{i\alpha} = \sum_j \rho_{ij} \left(H_{ij}^{(\alpha 0)} - \sum_{kl} S_{ik}^{el} S_{ik}^{(\alpha 0)} S_{kl}^{-1} H_{lj} \right) \quad . \tag{39}$$

In order to form an equation of motion for the electronic functions, $\dot{B}_j$ in Eq. (32) must first be substituted:

$$\sum_j i\rho_{ij} S_{ij}^{g} |\dot{\psi}_j\rangle = \sum_j \left(\rho_{ij} H_{ij}^{g} - i\rho_{ij}\tau_{ij}^{g} \right.$$
$$\left. - \sum_{kl} \rho_{il} S_{ij}^{g} S_{jk}^{-1} \left(H_{kl} - iS_{kl}^{el}\tau_{kl}^{g} - iS_{kl}^{g}\tau_{kl}^{el} \right) \right) |\psi_j\rangle \tag{40}$$

and then re-arranged to give

$$i|\dot{\psi}_k\rangle = \sum_{ij} (\rho_{ki} S_{ki}^{g})^{-1} \left[\rho_{ij} \left((H_{ij}^{g} - i\tau_{ij}^{g}) - \sum_{lm} S_{il}^{g}|\psi_l\rangle S_{lm}^{-1}\langle\psi_m| (H_{mj}^{g} - i\tau_{mj}^{g}) \right) \right.$$
$$\left. + \sum_{lm} i\rho_{im} S_{ij}^{g} S_{jl}^{-1} S_{lm}^{g} \tau_{lm}^{el} \right] |\psi_j\rangle \quad . \tag{41}$$

As they are simply reformulations of the single-set vMCG EOMS, Eqs. (36),(37) and (41) are exact solutions of the TDSE that can connect full quantum dynamics to Ehrenfest dynamics. In this context these equations have been presented in a recent feature article [44].

To solve (36),(37) and (41) would require substituting τ^g in Eq. (41) using the EOM for the GBF parameters in from Eq. (37), then choosing an appropriate expression for the (non-Hermitian) matrix τ^{el}. Rather than doing this, we note that if we ignore the off-diagonal overlap elements of S_{ij}^g, τ_{ij}^g and H_{ij}^g in Eq. (41), the electronic functions de-couple from each other and lead to

$$i|\dot{\psi}_k\rangle = \left(H_{kk}^g - H_{kk} + i\tau_{kk}^{el}\right)|\psi_k\rangle \quad . \tag{42}$$

The rationale for ignoring these off-diagonal terms is that if the GBFs are sufficiently narrow they will be small. By introducing this approximation the EOM are no longer variational but still a full solution of the TDSE, if the basis set is large enough.

If the centre of GBF g_k is q_k, then

$$H_{kk}^g = \langle g_k|H|g_k\rangle = \langle T_N\rangle_{kk} + H_{el}(q_k) \tag{43}$$

where $\langle T_N\rangle_{kk}$ is the kinetic energy of the GBF and $H_{el}(q_k)$ is the electronic Hamiltonian at q_k. The energy for the configuration k can now be written as two parts

$$\langle g_k\psi_k|H|g_k\psi_k\rangle = \langle T_N\rangle_{kk} + \langle\psi_k|H_{el}(q_k)|\psi_k\rangle \quad . \tag{44}$$

Remembering that the on-diagonal elements of $\boldsymbol{\tau}$ can be defined by any real number we choose

$$i\tau_{kk}^{el} = \langle\psi_k|H_{el}(q_k)|\psi_k\rangle \tag{45}$$

leading to the simple EOM for the electronic functions:

$$i|\dot{\psi}_k\rangle = H_{el}(q_k)|\psi_k\rangle \quad . \tag{46}$$

This is Ehrenfest dynamics. The electronic function evolves under the Hamiltonian that follows the centre of the GBF. However, due to the variational EOM for the GBFs of Eq. (37) the nuclear trajectories are not classical. We will refer to this as the variational Ehrenfest multi-configurational Gaussian (veMCG) method as, although the electronic functions are not variational, the nuclear functions and expansion coefficients are.

To decouple the electronic and nuclear part fully to provide a practical computational scheme, we will follow the clMCG level and retain only the classical terms in the GBF EOM. We then obtain the Ehrenfest multi-configurational Gaussian (eMCG) method.

$$i\dot{B}_k = \sum_{ij} S_{ki}^{-1}\left(H_{ij} - iS_{ij}^{el}\tau_{ij}^g - iS_{ij}^g\tau_{ij}^{el}\right)B_j \tag{47}$$

$$\dot{\xi}_{k\alpha} = -2\zeta_{k\alpha}\frac{p_{k\alpha}}{m} - i\frac{\partial V}{\partial x_\alpha}\Big|_{\mathbf{x}=\mathbf{q}} \tag{48}$$

$$i|\dot{\psi}_k\rangle = H_{el}(q_k)|\psi_k\rangle \quad . \tag{49}$$

These are equivalent to the multi-configuration Ehrenfest (MCE) equations of motion of Shalashilin and co-workers [47], which were obtained from a different approach. The implementation details also differ.

Finally, if we also ignore the off-diagonal matrix elements in Eq. (36) this leads to

$$i\dot{B}_k = \left(H_{kk} - i\tau_{kk}^g - i\tau_{kk}^{el}\right) B_k \tag{50}$$

As the configurations are now independent this is a phase that is associated with each classical trajectory. The matrix elements H_{kk} and τ_{kk}^{el} are given but τ_{kk}^g can now be chosen. Different values merely move as to where this phase is propagated, as part of the expansion coefficient or as the phase of the GBF. In Vacher et al [44] the choice

$$i\tau_{kk}^g = H_{kk} \tag{51}$$

was made. Alternatively, using the usual vMCG choice

$$i\tau_{kk}^g = 0 \tag{52}$$

results in

$$i\dot{B}_k = \langle g_k | T_N | q_k \rangle \quad . \tag{53}$$

The iMCG level of theory is thus equivalent to a multi-configurational Ehrenfest ansatz. The iMCG expansion coefficients, A_{ks}, are then the electronic function coefficients, c_{ks}, with a (time-dependent) normalisation factor, B_k, for each trajectory.

2.4. Model Hamiltonian

The allene radical cation has five low lying states. Of interest here is the $\tilde{A}(^2E)/\tilde{B}(^2B_2)$ manifold. A vibronic-coupling model Hamiltonian has been set up for this molecule previously, incorporating the coupling between these states, to simulate the photo-electron spectrum [48]. Neutral allene at the ground-state equilibrium geometry has D_{2d} symmetry. As a result the doubly degenerate $\tilde{A}$ state is subject to the rare $e \otimes B$ Jahn-Teller distortion, whereby the degeneracy is lifted by vibrations with B_1 and B_2 symmetry. This state is further pseudo-Jahn-Teller coupled to the $\tilde{B}$ state via doubly-degenerate E vibrations.

The vibronic coupling model uses a diabatic electronic basis, i.e. the kinetic energy operator is diagonal and coupling between the states appears as off-diagonal functions in the potential operator matrix. The nuclear coordinates used for allene are the ground-state mass-frequency scaled normal mode vibrations. A low-order Taylor series is then used to express the potential functions. From symmetry considerations, in the $\tilde{A}$ state the three B_2 modes provide the linear on-diagonal coupling terms, and the one B_2 vibration the off-diagonal.

To first-order, the Hamiltonian matrix can thus be written

$$
\begin{aligned}
\mathbf{H} \;=\; & \sum_{i=1}^{15} \frac{\omega_i}{2}\left(-\frac{\partial^2}{\partial Q_i^2}+Q_i^2\right)\mathbf{1} + \begin{pmatrix} E_E & 0 & 0 \\ 0 & E_E & 0 \\ 0 & 0 & E_{B_2} \end{pmatrix} \\
& + \begin{pmatrix} \sum_{i=1}^{3}\kappa_i Q_i & 0 & 0 \\ 0 & \sum_{i=1}^{3}\kappa_i Q_i & 0 \\ 0 & 0 & \sum_{i=1}^{3}\kappa_i' Q_i \end{pmatrix} \\
& + \begin{pmatrix} \sum_{i=5}^{7}\lambda_i Q_i & \lambda_4 Q_4 & \sum_{i=8}^{11}\lambda_i' Q_{ix} \\ \lambda_4 Q_4 & \sum_{i=5}^{7}-\lambda_i Q_i & \sum_{i=8}^{11}\lambda_i' Q_{iy} \\ \sum_{i=8}^{11}\lambda_i' Q_{ix} & \sum_{i=8}^{11}\lambda_i' Q_{ix} & 0 \end{pmatrix} \quad (54)
\end{aligned}
$$

The modes are defined in Table 2, with Q_i the normal mode for vibration ν_i. The full model is expanded to second order. See Ref. [48] for details and the values of the parameters.

At the Franck-Condon point, $\mathbf{Q} = 0$ (termed Q_0), the doubly-degenerate $\tilde{A}$ state forms a Jahn-Teller conical intersection, with the degeneracy lifted on the diagonal elements of the Hamiltonian matrix by the three B_2 modes. The degeneracy is lifted in the off-diagonal, coupling, Hamiltonian element by the B_1 mode. This is the torsional mode with the end H–C–H units rotating towards each other. The diabatic surfaces along the $Q_7(B_2)$ vibration are shown in Fig. 1 (a) with the torsion at $45°$. Along this mode the diabatic curves for the $\tilde{A}$ state cross and the degenerate point in the can be seen at $\mathbf{Q} = 0$, with the Jahn-Teller splitting resulting in the two wells labeled $\tilde{A}_L$ and $\tilde{A}_R$. The adiabatic surfaces, the eigenvalues of the Hamiltonian taking the coupling into account, are shown in Fig. 1(b). These doublet states are labeled D_2 - D_4 as D_0 and D_1 are in the lower energy $\tilde{X}$ band.

The $\tilde{X}$ state of the radical cation is due to ionisation from the degenerate highest occupied molecular orbitals (HOMO). The $\tilde{A}$ state of the radical cation is from ionisation out of the degenerate HOMO-1 pair, and the $\tilde{B}$ state the HOMO-2. The HOMO-1 and HOMO-2 orbitals at the Franck-Condon point are shown in Fig. 1(c)(i)-(iii). The HOMO-1 pair are each localised on one H–C–H group. Ionisation of allene thus creates an electron "hole" in one end of the molecule. The character of the molecular orbital (MO) is retained moving along the Jahn-Teller active B_2 modes and these orbitals thus define the diabatic basis. Movement along the B_1 mode couples the two states. The HOMO-1 pair at a torsion angle of $45°$ are shown in Fig. 1(c)(iv),(v). The conjugation along the chain due to the coupling leads to population transfer between the states, that corresponds to charge being transferred between the ends of the molecule.

Charge migration takes place when the charge moves without nuclear motion. If the molecule remains at Q_0, this does not occur as the coupling is zero. However if the molecule is twisted away from the equilibrium geometry along the B_1 torsion mode, the diabatic coupling means that the eigenfunctions of the ion are a superposition of the states populated by ionisation from the neutral. Consequently, if the neutral degenerate states are labeled ψ_L and ψ_R, the ion
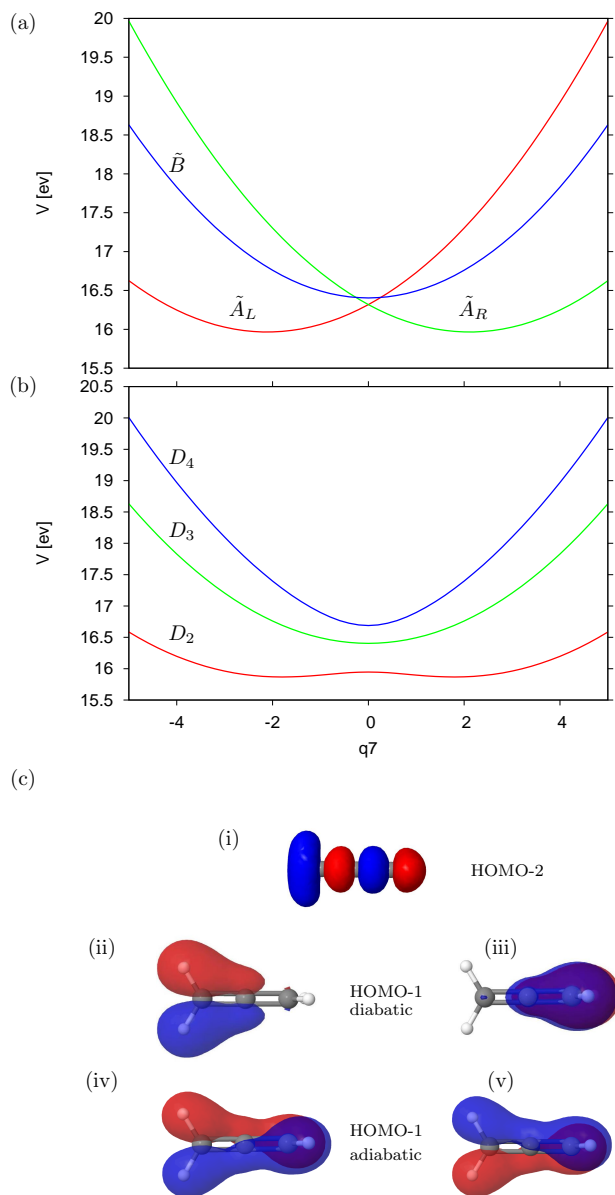
Figure 1: The (a) diabatic and (b) adiabatic potential energy surfaces for the allene radical cation model Hamiltonian along the $Q_7(B_2)$ vibrational coordinate with the torsion angle kept at $45°$. (c) Molecular orbitals (MOs) for the neutral allene molecule. (i) the HOMO-2 (ii), (iii) the degenerate HOMO-1 pair at the equilibrium geometry with D_{2d} symmetry. (iv), (v) the HOMO-1 pair at a geometry twisted by $45°$ away from the equilibrium geometry. Ionisation from (i), (ii), (iii) define the $\tilde{B}$, $\tilde{A}_L$ and $\tilde{A}_R$ diabatic states respectively. (iv), (v) show the conjugation obtained at $45°$ due to the non-adiabatic coupling.

14

Table 2: Definitions and descriptions of the 15 vibrational modes in the allene molecule. Frequencies are for the ground-state calculated at the MP2/cc-pVTZ level. N are the number of harmonic oscillator DVR functions used in the MCTDH calculations, and n the number of multi-dimensional single particle functions with the combination of modes included by the bracket.

Label	Frequency (cm^{-1})	Description	MCTDH basis set	
			N	n
$\nu_1(A_1)$	3015	HCH sym str	24	} 13
$\nu_2(A_1)$	1443	HCH in-phase bend	32	
$\nu_3(A_1)$	1072	CCC sym str	32	} 14
$\nu_4(B_1)$	865	HCCH torsion	32	
$\nu_5(B_2)$	3407	HCH oo-phase str	10	
$\nu_6(B_2)$	1957	CCC anti-sym str	10	} 17
$\nu_7(B_2)$	1398	HCH oo-phase bend	30	
$\nu_8(E)$	3486	HCH anti-sym str	10	
$\nu_9(E)$	999	HCH rock	18	
$\nu_{10}(E)$	841	HCH wag	12	} 1
$\nu_{11}(E)$	355	CCC bend	8	

state can be written

$$\psi_+ = c_L(t)\psi_L + c_R(t)\psi_R \quad . \tag{55}$$

If the ionisation removes the electron from ψ_L then at $t = 0$ the coefficients are $c_L(0) = 1$ and $c_R(0) = 0$. The coefficients evolve according to Rabi-like oscillations due to the coupling, and charge migration occurs. The MOs of the cation at a torsion angle of 45° are shown in the lower panel of Fig. 1 along with the adiabatic surfaces showing how the coupling leads to conjugation along the chain allowing the charge migration.

The model has the useful property that the strength of the coupling governing the charge migration is controlled by changing the torsion angle - the wider the angle the stronger the coupling. By comparison of the dynamics of static nuclei to that of moving nuclei after photo-ionisation starting at a particular angle, the diabatic state populations of this simple model can thus be used to observe the signature of charge migration in charge transfer.

The need for an initial controlled twisting of the neutral molecule is not an easily realizable situation for allene ionisation, but the ubiquitous nature of the vibronic coupling model means that similar behaviour can be found in other systems in which the twist is not required to provide the coupling. For example, in studies using Ehrenfest trajectories on the ionisation in aromatic molecules, a distortion from the equilibrium geometry was required to see charge migration in benzene, but it happens spontaneously in toluene and para-xylene [45], as it does in the non-aromatic bismethylene-adamantane [46]."

3. Results of Simulations

3.1. Charge Migration v Charge Transfer

Using the model Hamiltonian of allene described above, two different sets of calculations were performed using full grid-based quantum dynamics and the MCTDH method. At the equilibrium geometry the torsion angle between the H–C–H groups is $90°$. By altering the torsion angle the initial wavepacket experiences coupling between the degenerate orbitals allowing charge migration to occur. The first calculations were started with a torsion angle of $75°$, giving a small coupling between the degenerate orbitals. The second calculations were started with a torsion angle of $45°$, giving a larger coupling. As the model is set up in normal mode coordinates, a change in torsion angle requires changing not only the coupling mode but also the totally symmetric modes to keep the bond lengths correct. In the mass-frequency scaled normal mode coordinates of the model, an angle of $75°$ corresponds to a coordinate of $(Q_1, Q_2, Q_3, Q_4) = (-0.1308, -0.0556, 0.0100, 1.2543)$ and an angle of $45°$ corresponds to a coordinate of $(Q_1, Q_2, Q_3, Q_4) = (-1.1635, -0.4945, 0.0892, 3.6774)$ with all other coordinates having a value of 0.

The initial wavepacket is centred at the starting geometry for each model, i.e. displaced from the Franck-Condon point, $\mathbf{Q}_0$, with the width appropriate for the neutral ground-state vibrational frequencies. The simulation is initiated by placing this packet in the second diabatic state, corresponding to making a hole at the right-hand end of the twisted molecule on ionisation. The population dynamics following this ionisation for both initial torsion angles are shown in Fig. 2. Coupling to the B-state was ignored as this plays no role in the charge migration.

Fig. 2 (a) and (e) show the charge migration dynamics for the two angles. This was calculated using the gMCG method with a single time-independent GBF, i.e. static nuclei. The state populations show a simple oscillation between the two ends of the molecule, with a period related to the coupling strength. The populations obtained from full quantum dynamics calculated using the MCTDH method allowing the nuclei to move are shown in Fig. 2 (b) and (f). The charge migration oscillations are damped, but the signal is still visible in the first 10 fs, particularly in the $\Theta = 45°$ model.

Fig. 2 (c) and (g) show the result calculated using the vMCG method with 50 GBFs. The MCTDH result is shown as a dotted line. The vMCG method is clearly able to describe the coupled nuclear and electronic dynamics of this system with a very small number of functions. The widths of the GBFs were taken as $1/\sqrt{2}$ in each direction. In the mass-frequency scaled coordinate system of the Hamiltonian, this corresponds to the width of the neutral ground-state wavepacket.

The final plots, Fig. 2 (d) and (h), show the result with a single GBF. This follows the Ehrenfest classical trajectory from the starting geometry. It is clearly unable to describe the nuclear dynamics correctly: the charge migration signal dominates and charge localisation occurs, with the dynamics ending at one end of the molecule rather than spread over the whole molecule as seen in

the quantum dynamics. Interestingly the charge is at different ends depending on the initial torsion angle.

To show the dynamics of the nuclei as the charge migration is damped in the model starting with a torsion angle of $\Theta = 45°$, the expectation values of the three most active vibrational modes are plotted in Fig. 3. These are the B_1 coupling torsional vibration, Q_4, and the lowest frequency modes in the A_1 and B_2 symmetries, Q_3 and Q_7 respectively. Results from the full quantum dynamics simulations and the classical Ehrenfest trajectory are shown. The motion followed by the wavepacket along the symmetric mode Q_3 is classical, while that along the B_2 Jahn-Teller active mode is clearly very non-classical. The reduced density along Q_7 is shown in Fig. 3 (d) shows the bifurcated waveform motion along this mode, something that a single classical trajectory cannot follow.

This model thus provides a hard test for a method in the description of coupled electronic-nuclear motion in a charge-transfer problem. The dynamics can be divided into the short-time (< 10 fs) when charge migration dominates and long-time (> 10 fs) when the nuclear motion leads to a permanent charge transfer.

3.2. Different Dynamics Model: Initial Conditions and Convergence

In the following, the different levels of theory laid out above will be used to see how well they can follow the coupled electronic-nuclear dynamics of the allene ionisation. When using the non-variational GBFs of the clMCG, iMCG and eMCG methods, the initial positions of the functions play a role in the dynamics, and for good results it is important to cover phase space. To make the results easier to converge, in the following only the three most important modes, Q_3, Q_4 and Q_7 will be included in the dynamics with the initial wavepacket kept stationary along the other modes. The initial wavepacket in all cases is that with $\Theta = 45°$.

The state populations as a function of time, calculated with different levels of theory, are shown in Fig. 4. In Fig. 4(a) the vMCG result with 30 GBFs is compared to the full quantum dynamics result (dotted line). The charge-migration and charge-transfer dynamics are very similar to those seen in the 15-dimensional calculations above, showing the dominance of the three selected modes on the nuclear dynamics. There is still a clear charge migration at short times with a full oscillation in under 10 fs before the long-time damping and accompanying charge transfer. Again, the accuracy of the vMCG method is very good, and fewer functions are needed than in the 15-dimensional calculation, indicating the smaller phase space that must be covered.

The best result obtained using classical GBFs in the clMCG level is shown, in Fig. 4(b), using 150 functions. With more functions the result did not noticeably improve while with fewer the populations contained stronger oscillations across the whole time range. The short-time charge migration dynamics was reproduced well in every case. In these calculations the initial positions of the GBFs were taken from a Wigner distribution of the ground-state neutral wavepacket. This should lead to faster convergence than simply taking random
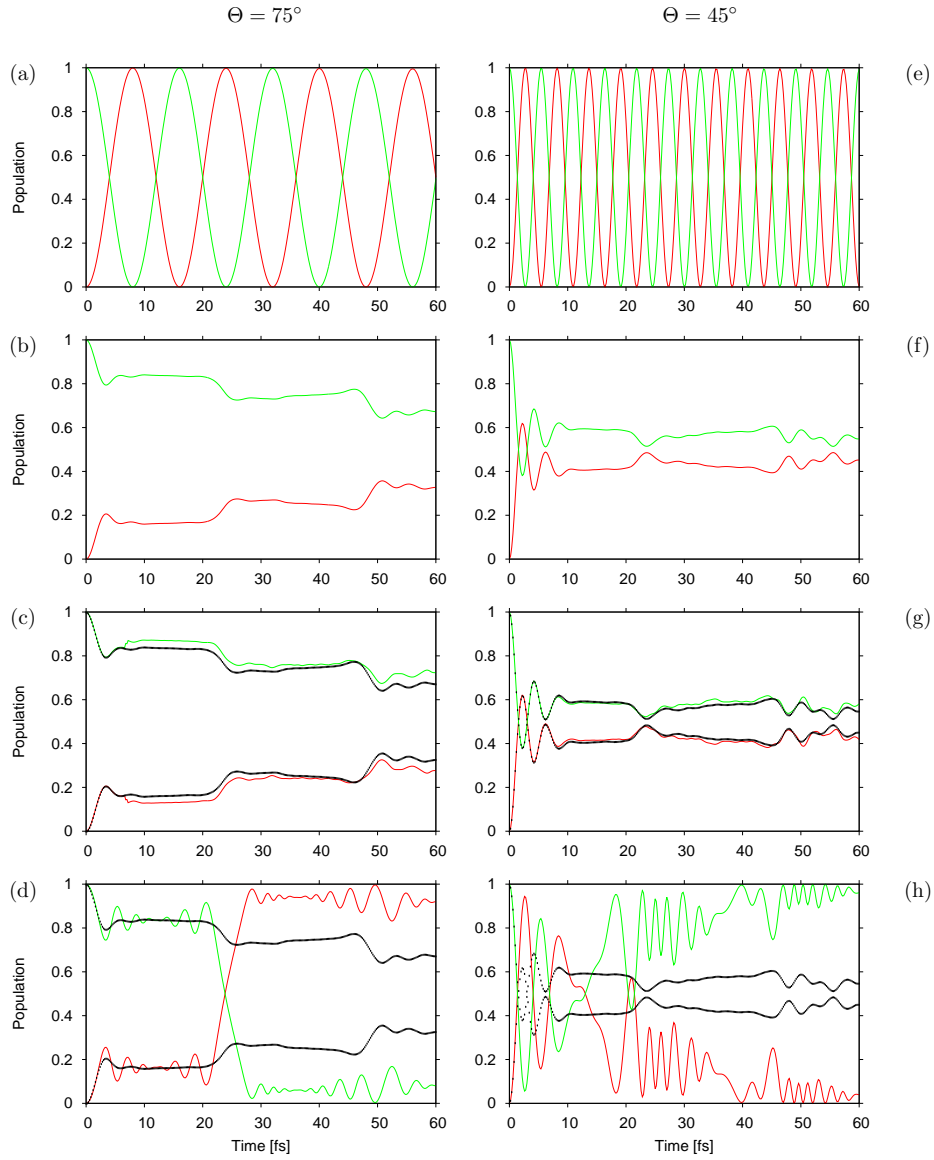
17

Figure 2: Population dynamics of allene after ionization on the right hand end of the molecule. In (a) - (d) the molecule had a torsional twist of $\Theta = 75°$ and in (e) - (h) the angle was $\Theta = 45°$. (a), (e) Charge migration with static nuclei. (b), (f) full quantum dynamics of charge migration and charge transfer using the MCTDH method. (c), (g) Full quantum dynamics using the vMCG method with 50 GBFs. The MCTDH result is the dotted line. (d), (h) Population dynamics with a single GBF, i.e. classical nuclei.
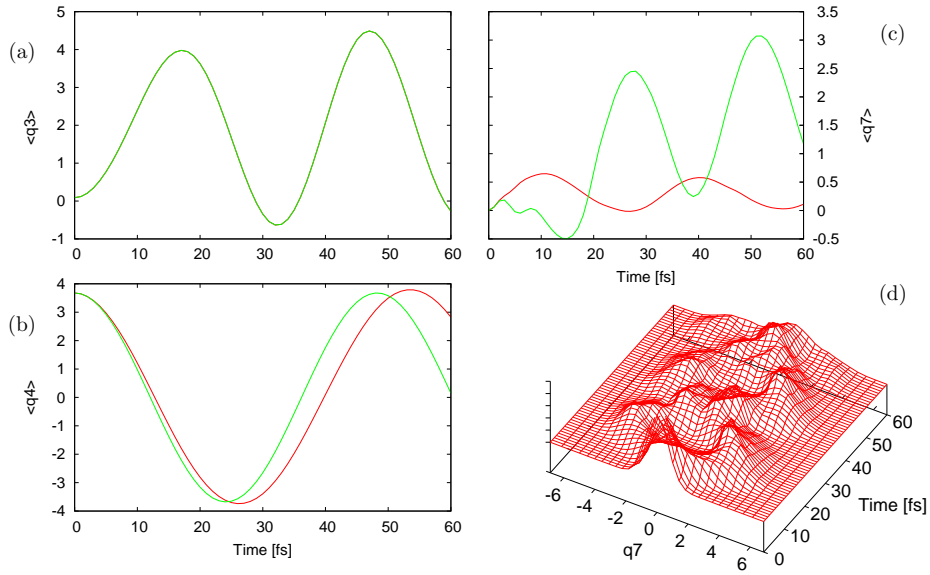
Figure 3: Expectation Values of the main vibrational coordinates (a) $\langle Q_3 \rangle$ (b) $\langle Q_4 \rangle$ (c) $\langle Q_7 \rangle$ from simulations starting with a torsion angle of $\Theta = 45°$. In green are the results from the MCTDH calculation, in red the classical Ehrenfest trajectory from the Franck-Condon point. (d) The reduced density along Q_7 is shown as a function of time.

positions in configuration space, and indeed it produced better results with fewer functions.

While more functions were required for convergence, a question is whether the simplicity of the clMCG equations makes the method preferable to vMCG. In this case, the computational cost is similar. On a single processor of a standard workstation, the 30 GBF vMCG calculation required 2535 s while the 150 GBF clMCG calculation slightly more at 3259 s. The majority of effort in the latter goes in to calculating the matrix elements and inverting the overlap matrix. For the 15-mode calculation of Sec. 3.1, the 50 GBF vMCG calculation required 13 hr 37 min on the same machine. A 100 GBF clMCG calculation of the same system require 11 hr 58 min, but was not close to convergence.

In the vMCG and previous clMCG calculation, the widths of the GBFs were taken as $1/\sqrt{2}$ in each direction. It may be advantageous to take narrower GBFs to, e.g. minimise the error due to using a local harmonic approximation in the calculation of the integrals. When using narrower GBFs a fit must be made of the initial wavepacket in the basis set. This was done by projecting the initial wavepacket on to the basis set, i.e. the initial coefficients were chosen by

$$A_{js} = \sum_b |g_j\rangle S_{jb}^{-1} \langle g_b|\psi(0)\rangle \tag{56}$$

with the index s set to be the initial state. When this is done more GBFs are required to cover phase space and the quality of the result drops. A calculation using the clMCG level with 200 GBFs with a width of 0.4 is shown in Fig. 4(c). It is not as close to the full result as the 150 wider GBFs. It should be noted that even with 200 GBFs the initial wavepacket is not exactly represented: the expectation values of the 3 modes are only approximately correct and the widths

19

along all modes are less than $1/\sqrt{2}$ in coordinate space and greater than $1/\sqrt{2}$ in momentum space.

In Fig. 4(d) the result from an iMCG calculation also with 200 GBFs is shown. Given the simple representation of the evolving wavepacket the result is remarkably good. The shape of the population transfer is correct, with the short-time dynamics well-reproduced, though the oscillations are slightly damped compared to the full result. The long-time dynamics are not exactly reproduced due to the lack of nuclear coherence. This allows crossings of population not seen in the full quantum result. The magnitude is, however, reasonable.

The iMCG method with narrow GBFs is close in spirit to a swarm of trajectory description of the wavepacket. In such calculations, trajectories do not have different weights but simply sample the Wigner distribution to provide the initial wavepacket. Fig. 4(e) shows the result from an iMCG calculation with 200 GBFs starting with equal weights. This means that the initial wavepacket is defined by the Wigner distribution rather than by fitting, and the wavepacket is described effectively by a swarm of tractories. The choice makes surprisingly little difference and shows that representing a wavepacket by many Ehrenfest trajectories selected from the Wigner function is a reasonable way to treat the system if the details of the later time propagation are not required.

The final calculation shown in Fig. 4(f) is the result from an eMCG simulation with 150 GBFs with widths of $1/\sqrt{2}$. For this simulation, 200 classical trajectories sampled from a Wigner distribution were initially run and the coordinates and momenta along with the Ehrenfest potentials and state populations for each stored. The eMCG basis functions were then run along these trajectories using spline fits of the data and the evolution of the expansion coefficients calculated. This is the procedure that could be used to run an eMCG simulation along Ehrenfest trajectories calculated by a quantum chemistry program, such as Gaussian, which have been generated and used in a number of studies on charge migration [25, 26, 27].

It was hoped that this method would give a quality similar to the clMCG, but while the initial decay and the period of the charge migration oscillations in the short-time dynamics is reproduced the oscillations are not correctly damped. This is probably due to the implementation. For example, the integrals only used the value of the potential at the centre rather than the full LHA.

4. Conclusions

We have presented a model Hamiltonian based on the ionisation of allene that displays the transition from charge migration to charge transfer. The charge migration is due to the contribution of the molecular orbital from which the electron is removed contributing to two different eigenstates of the ion. Two models were set up, with the molecule twisted by different amounts leading to strong and weak coupling between the electronic states. Charge transfer is then due to the motion of the nuclei resulting ultimately in an equilibrated charge distribution.
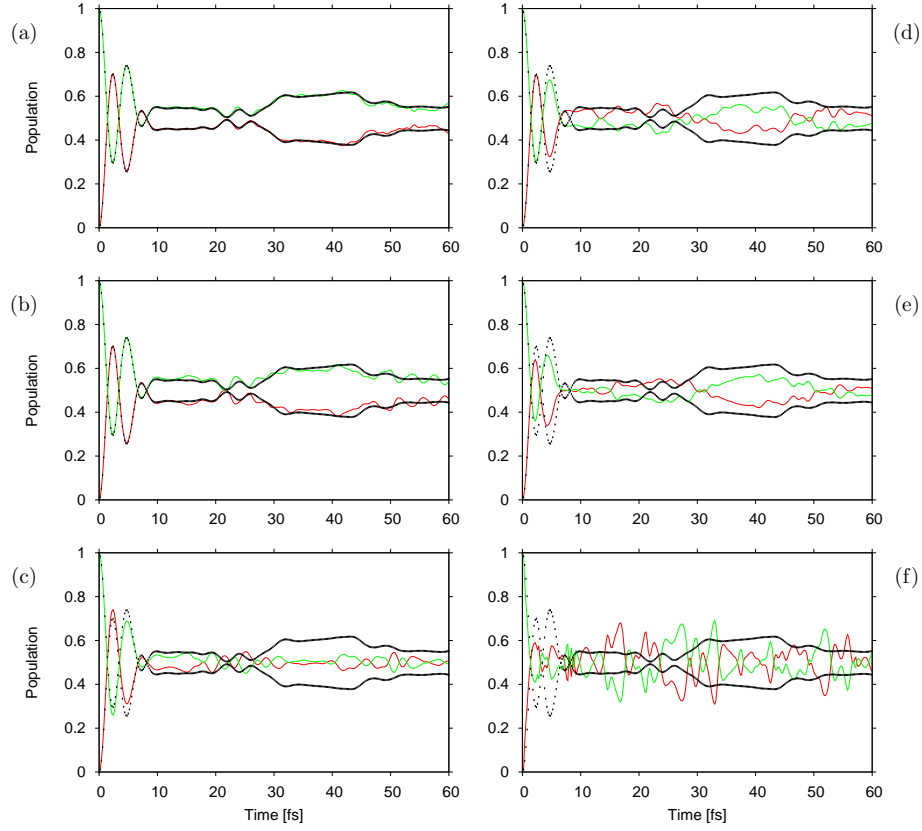
Figure 4: Population dynamics of allene with a torsion angle of $\Theta = 45°$ after ionization on the right hand end of the molecule calculated using different levels of theory and including only the main modes, Q_3, Q_4 and Q_7 in the dynamics. (a) The vMCG method with 30 variational GBFs with a width $1/\sqrt{2}$. (b) The clMCG method with 150 classical GBFs with a width $1/\sqrt{2}$ (c) The clMCG method with 200 classical GBFs with a width 0.4. (d) The iMCG method with 200 independent classical GBFs with a width 0.4 (e) The iMCG method with 200 independent classical GBFs with a width 0.4 and initial equal weights (f) The eMCG method with 150 classical GBFs with a width $1/\sqrt{2}$ In the iMCG, clMCG and eMCG calculations the initial GBFs were taken from a Wigner distribution. The full quantum result is shown in all plots as a dotted line.

21

It both case the charge migration is seen as a fast oscillation of population between the orbitals located on either end of the molecule, moving over the static nuclear framework. The oscillation period is proportional to the coupling strength. The migration is damped by the nuclear motion, and in the weaker coupling model is barely visible in the population dynamics of the coupled electronic-nuclear dynamical system. In the strong coupling model, with an initial torsion angle of 45°, the migration is fast enough to still be visible in the populations before the nuclear motion starts to dominate.

In this model, an analysis of the the nuclear dynamics shows a bifurcation of the nuclear wavepacket along one mode due to the non-adiabatic coupling between the states. A single classical Ehrenfest trajectory is unable to follow this motion and cannot reproduce the state populations. This makes the model suitable as a benchmark system for quantum dynamics methods as the nuclear coherence plays an important role in the dynamics. It is also accessible to full quantum dynamics methods using the MCTDH method which can be used to provide an exact comparison.

Different levels of theory based on Gaussian Wavepacket methods have been presented as a hierarchy that may prove useful in quantum dynamics studies as they have different levels of computational effort, along with different convergence behaviours. The vMCG method is a full solution of the TDSE with a variational basis set. It reproduces the full result with a small number of function. The clMCG method uses a non-variational basis set of Gaussian functions that follow classical trajectories, but still can provide the full solution of the TDSE with enough functions. It is seen, however, that many more functions are needed to follow the dynamics than vMCG, and this may outweigh the ease of propagating the functions. The converged 3-mode clMCG calculation took more time than the corresponding vMCG result, while a converged 15-mode result was not obtained using clMCG due to the effort required.

A second point to be noted is that the convergence performance of vMCG is independent of the choice of GBF initial positions. This is due to the variational nature of the GBF evolution which means that they adjust to produce the same result (within numerical error) for a given number of functions irrespective of starting positions. This is not the case for classical GBFs whose trajectories are determined by the initial positions (and momenta) so adding functions may or may not improve a result depending on how they are placed at the start. This gives vMCG a practical advantage.

Removing the coupling between the basis functions results in the iMCG method, which is effectively a swarm of weighted classical trajectories with a Gaussian function. This is not a full solution of the TDSE, and it is seen that the method can only approximately follow the system dynamics. It does, however, provide the main features such as the time-scale for the charge migration damping.

In this study pre-computed potentials and couplings are used. If the integrals required are made using the LHA, methods based on GBFs can also be used in direct dynamics studies in which the potentials are calculated on-the-fly using quantum chemistry calculations as the wavepacket evolves in time [19, 20, 21].

These, however, become less tractable if a large number of states need to be included due to the number of couplings that must be calculated. An alternative to this is provided by a multi-configurational Ehrenfest approach, in which a time-dependent electronic basis set provides a single time-dependent potential surface for the nuclei. This may provide a new route to efficient direct dynamics simulations as they can be coupled with Ehrenfest trajectories provided by quantum chemistry calculations.

To connect the vMCG method and the MCE approach, variational EOMs were set up for the full problem with time-dependent electronic functions. If the overlaps between the nuclear basis functions are ignored in the time-evolution of the electronic functions, these are propagated by the electronic Hamiltonian defined at the centre of the associated nuclear function. These functions then provide the Ehrenfest potentials for the nuclear motion, which may either follow variational (evMCG) or classical (eMCG) trajectories. In both of these methods a full solution of the TDSE is in principle possible. In simulations using the eMCG method, however, approximations introduced in the implementation meant that it was found to overdamp the charge migration oscillations. Finally, a set of classical Ehrenfest trajectories ignoring the coupling between the nuclear functions was shown to be equivalent to the iMCG method.

In summary, the work presented here provides a basis for testing methods aiming at calculating the coupled electronic-nuclear motion in charge migration problems. It shows that direct dynamics at the vMCG level are capable of reproducing the full quantum dynamics result with a small basis set, while even the cheaper Ehrenfest-trajectory based iMCG, is capable of capturing the main physics involved. Further development will try to improve on the efficiency and accuracy that can be obtained by the Ehrenfest methods by, e.g. improving on the calculation of the integrals.

References

[1] L. Cederbaum, J. Zobeley, Ultrafast charge migration by electron correlation, Chem. Phys. Lett 307 (1999) 205–210.

[2] A. L. Kuleff, L. S. Cederbaum, Ultrafast correlation-driven electron dynamics, J. Phys. B 47 (2014) 124002. doi:10.1088/0953-4075/47/12/124002.

[3] S. Lünnemann, A. I. Kuleff, L. S. Cederbaum, Ultrafast charge migration in 2-phenylethyl-N,N-dimethylamine, Chem. Phys. Lett. 450 (2008) 232–235. doi:10.1016/j.cplett.2007.11.031.

[4] A. L. Kuleff, S. Lünnemann, L. S. Cederbaum, Electron-correlation-driven charge migration in oligopeptides, Chem. Phys. 414 (2013) 100–105. doi:10.1016/j.chemphys.2012.02.019.

[5] N. V. Golubev, A. I. Kuleff, Control of charge migration in molecules by ultrashort laser pulses, Phys. Rev. A 91 (2015) 51401. doi:10.1103/PhysRevA.91.051401.

[6] R. Weinkauf, P. Aicher, G. Wesley, J. Grotemeyer, E. W. Schlag, Femtosecond versus Nanosecond Multiphoton Ionization and Dissociation of Large Molecules, J. Phys. Chem. 98 (1994) 8381–8391. doi:10.1021/j100085a019.

[7] F. Remacle, R. D. Levine, An electronic time scale in chemistry., PNAS 103 (2006) 6793–6798. doi:10.1073/pnas.0601855103.

[8] F. Calegari, D. Ayuso, A. Trabattoni, L. Belshaw, S. De Camillis, S. Anumula, F. Frassetto, L. Poletto, A. Palacios, P. Decleva, J. B. Greenwood, F. Martin, M. Nisoli, Ultrafast electron dynamics in phenylalanine initiated by attosecond pulses, Science. 346 (2014) 336–339.

[9] C. Cerjan (Ed.), Numerical Grid Methods and their Application to Schrödinger's Equation, Kluwer Academic Publishers, Dordrecht, 1993.

[10] R. Kosloff, Quantum Molecular Dynamics on Grids, in: R. E. Wyatt, J. Z. H. Zhang (Eds.), Dyn. Mol. Chem. React., Marcel Dekker, New York, 1996, pp. 185–230.

[11] H.-D. Meyer, U. Manthe, L. S. Cederbaum, The Multi-Configurational Time-Dependent Hartree Approach, Chem. Phys. Lett. 165 (1990) 73–78.

[12] M. H. Beck, A. Jäckle, G. A. Worth, H.-D. Meyer, The multiconfiguration time-dependent Hartree method: A highly efficient algorithm for propagating wavepackets., Phys. Rep. 324 (2000) 1–105.

[13] H.-D. Meyer, F. Gatti, G. A. Worth (Eds.), High dimensional quantum dynamics: Basic Theory, Extensions, and Applications of the MCTDH method, VCH, Weinheim, Germany, 2008.

[14] H. Wang, M. Thoss, Multilayer formulation of the multiconfiguration time-dependent Hartree theory, J. Chem. Phys. 119 (2003) 1289–1299.

[15] O. Vendrell, H.-D. Meyer, Multilayer multiconfiguration time-dependent Hartree method: implementation and applications to a Henon-Heiles hamiltonian and to pyrazine., J. Chem. Phys. 134 (2011) 044135–15. doi:10.1063/1.3535541.

[16] G. A. Worth, H.-D. Meyer, H. Köppel, L. S. Cederbaum, I. Burghardt, Using the MCTDH wavepacket propagation method to describe multimode non-adiabatic dynamics, Int. Rev. Phys. Chem. 27 (2008) 569–606. doi:10.1080/01442350802137656.

[17] R. Borrelli, M. Thoss, H. Wang, W. Domcke, Quantum dynamics of electron-transfer reactions: photoinduced intermolecular electron transfer in a porphyrinquinone complex, Mol. Phys. 110 (2012) 751–763. doi:10.1080/00268976.2012.676211.

[18] G. A. Worth, M. A. Robb, Applying direct molecular dynamics to non-adiabatic systems, Adv. Chem. Phys. 124 (2002) 355–432.

[19] M. Ben-Nun, T. J. Martínez, *Ab Initio* Quantum Molecular Dynamics, Adv. Chem. Phys. 121 (2002) 439–512.

[20] K. Saita, D. V. Shalashilin, On-the-fly ab initio molecular dynamics with multiconfigurational Ehrenfest method., J. Chem. Phys. 137 (2012) 22A506-8. doi:10.1063/1.4734313.

[21] G. A. Worth, M. A. Robb, I. Burghardt, A novel algorithm for non-adiabatic direct dynamics using variational Gaussian wavepackets, Faraday Discuss. 127 (2004) 307–323. doi:10.1039/b314253a.

[22] I. Burghardt, H.-D. Meyer, L. S. Cederbaum, Approaches to the approximate treatment of complex molecular systems by the multiconfiguration time-dependent Hartree method, J. Chem. Phys. 111 (7) (1999) 2927–2938. doi:10.1063/1.479574.

[23] G. A. Worth, I. Burghardt, Full quantum mechanical molecular dynamics using Gaussian wavepackets, Chem. Phys. Lett. 368 (2003) 502–508.

[24] G. W. Richings, I. Polyak, K. E. Spinlove, G. A. Worth, I. Burghardt, B. Lasorne, Quantum dynamics simulations using Gaussian wavepackets: the vMCG method, Int. Rev. Phys. Chem. 34 (2015) 269–308. doi:10.1080/0144235X.2015.1051354.

[25] D. Mendive-Tapia, M. Vacher, M. J. Bearpark, M. A. Robb, Coupled electron-nuclear dynamics: charge migration and charge transfer initiated near a conical intersection., J. Chem. Phys. 139 (2013) 44110. doi:10.1063/1.4815914.

[26] M. Vacher, M. J. Bearpark, M. A. Robb, Communication: Oscillating charge migration between lone pairs persists without significant interaction with nuclear motion in the glycine and Gly-Gly-NH-CH3 radical cations, J. Chem. Phys. 140 (2014) 201102. doi:10.1063/1.4879516.

[27] M. Vacher, J. Meisner, D. Mendive-Tapia, M. J. Bearpark, M. A. Robb, Electronic Control of Initial Nuclear Dynamics Adjacent to a Conical Intersection, J. Phys. Chem. A 119 (2014) 5165–5172. doi:10.1021/jp509774t.

[28] D. V. Shalashilin, Quantum mechanics with the basis set guided by Ehrenfest trajectories: theory and application to spin-boson model., J. Chem. Phys. 130 (2009) 244101–244111. doi:10.1063/1.3153302.

[29] D. V. Shalashilin, Multiconfigurational Ehrenfest approach to quantum coherent dynamics in large molecular systems, Farad. Discuss. 153 (2011) 105–116. doi:10.1039/c1fd00034a.

[30] G. A. Worth, L. S. Cederbaum, Electron Transfer Along a Conjugated Chain: The Allene Radical Cation, Chem. Phys. Lett. 348 (2001) 477–482.

[31] A. Markmann, G. A. Worth, L. S. Cederbaum, Allene and pentatetraene cations as models for intramolecular charge transfer: vibronic coupling Hamiltonian and conical intersections., J. Chem. Phys. 122 (2005) 144320. doi:10.1063/1.1867433.

[32] T. J. Martínez, M. Ben-Nun, R. D. Levine, Multi-Electronic-State Molecular Dynamics: A Wave Function Approach with Applications, J. Phys. Chem. 100 (1996) 7884–7895.

[33] D. V. Shalashilin, M. S. Child, The phase space CCS approach to quantum and semiclassical molecular dynamics for high-dimensional systems, Chem. Phys. 304 (1-2) (2004) 103–120. doi:10.1016/j.chemphys.2004.06.013.

[34] S. Habershon, Linear dependence and energy conservation in Gaussian wavepacket basis sets, J. Chem. Phys. 136 (1) (2012) 14108–14109. doi:10.1063/1.3671978.

[35] Y. Wu, V. S. Batista, Matching-pursuit for simulations of quantum processes, J. Chem. Phys. 118 (2003) 6720–6724. doi:10.1063/1.1560636.

[36] W. Koch, T. J. Frankcombe, Basis expansion leaping: A new method to solve the time-dependent schrödinger equation for molecular quantum dynamics, Phys. Rev. Lett. 110 (2013) 263202–263205. doi:10.1103/PhysRevLett.110.263202.

[37] S. Garaschuk, J. Jakowski, V. A. Rassalov, Approximate quantum trajectory dynamics for reactive processes in condensed phases. Mol. Sim. 41 (2015) 86–106. doi:10.1080/08927022.2014.907493.

[38] B. F. E. Curchod, U. Rothlisberger, I. Tavernelli. Trajectory-based nonadiabatic dynamics with time-dependent density functional theory. ChemPhysChem. 14 (2013) 1314–1340. doi:10.1002/cphc.201200941.

[39] A. Abedi, N. T. Maitra, E. K. U. Gross, Exact Factorization of the Time-Dependent Electron-Nuclear Wave Function, Phys. Rev. Lett. 105 (12) (2010) 123002. doi:10.1103/PhysRevLett.105.123002.

[40] L. S. Cederbaum, The exact molecular wavefunction as a product of an electronic and a nuclear wavefunction, J. Chem. Phys. 138 (2013) 224110–224117. doi:10.1063/1.4807115.

[41] H.-D. Meyer, F. Gatti, G. A. Worth (Eds.), M C T D H: Basic Theory, Extensions, and Applications to Multidimensional Quantum Dynamics, VCH, Weinheim, Germany, 2009.

[42] I. Burghardt, M. Nest, G. A. Worth, Multiconfigurational system-bath dynamics using gaussian wavepackets: Energy relaxation and decoherence induced by a finite-dimensional bath, J. Chem. Phys. 119 (2003) 5364–5378.

[43] E. J. Heller, Time-dependent approach to semiclassical dynamics, J. Chem. Phys. 62 (1975) 1544–1555. doi:10.1063/1.430620.

[44] M. Vacher, M. J. Bearpark, M. A. Robb, Direct methods for non-adiabatic dynamics: connecting the single-set variational multi- configuration gaussian (vMCG) and ehrenfest perspectives, Theor Chem Acc 135 (2016) 187–197. doi:10.1007/s00214-016-1937-2.

[45] M. Vacher, D. Mendive-Tapia, M. J. Bearpark, M. A. Robb, Electron dynamics upon ionization: Control of the timescale through chemical substitution and effect of nuclear motion, J. Chem. Phys. 142 (2015) 094105. doi:10.1063/1.4913515.

[46] M. Vacher, F. E. A. Albertani, A. J. Jenkins, I. Polyak, M. J. Bearpark, M. A. Robb, Electron and nuclear dynamics following ionisation of modified bismethylene-adamantane, Farad. Discuss. (2016) In Press doi:10.1039//c6fd00067c.

[47] D. V. Shalashilin, Nonadiabatic dynamics with the help of multiconfigurational Ehrenfest method: Improved theory and fully quantum 24D simulation of pyrazine., J. Chem. Phys. 132 (2010) 244111. doi:10.1063/1.3442747.

[48] S. Mahapatra, G. A. Worth, H.-D. Meyer, L. S. Cederbaum, H. Köppel, The $\tilde{A}^2\mathrm{E}/\tilde{B}^2\mathrm{B}_2$ photoelectron bands of allene beyond the linear coupling scheme: An *ab initio* dynamical study including all fifteen vibrational modes., J. Phys. Chem. A 105 (2001) 5567–5576.